


Diffusion, relaxation, and aging of liquid and amorphous selenium

H. R. Schober ^{*}

Peter Grünberg Institut PGI-2 and JARA-HPC, Forschungszentrum Jülich, D-52425 Jülich, Germany



(Received 29 October 2020; revised 24 February 2021; accepted 26 February 2021; published 23 March 2021)

Relaxation and aging rates of amorphous selenium and its undercooled melt are calculated by molecular dynamics based on an interaction model derived from density functional calculations. After a fast initial relaxation immediately following the quench, the decrease of diffusivity and the simultaneous increase of dynamic heterogeneity follow an exponential law given by defect annihilation. As observed previously in a Lennard-Jones glass, the non-Arrhenius aging of atomic volume and energy is determined by the time dependence of the diffusivity. The aging time is determined for long times by the diffusivity and diverges exponentially with decreasing temperature. Amorphous selenium differs from metallic glasses in that the breaking of covalent bonds is important for the long time decay of the intermediate self-scattering function (ISSF). Surprisingly for the temperatures investigated, aging of the relaxation times of the ISSF and the bond decay follow the aging of the diffusivity.

DOI: [10.1103/PhysRevB.103.094202](https://doi.org/10.1103/PhysRevB.103.094202)

I. INTRODUCTION

When a liquid is quenched, the atomic motion slows and its relaxation rates decrease, as seen, for example, in the viscosity. Crystallization at the melting point T_m can be avoided by a sufficiently rapid quench, which leads to an undercooled or supercooled liquid that is metastable with respect to the crystal. Eventually it leaves thermodynamic equilibrium at a temperature where the relaxation rate is roughly equal to the quench rate. If the quench is stopped at lower temperatures, the liquid relaxes towards equilibrium, a process known as aging. Since relaxations generally slow upon cooling, so does aging. Studies on aging have a long history [1], and recent reviews cover metallic [2] and network glasses [3].

The slowing down of the relaxation rate is often used to define the glass transition temperature T_g ; $\eta(T_g) = 10^{12}$ Pa s, where η is the viscosity. Despite relaxation times exceeding 1000 ps below T_g , the glass relaxes (ages) at these temperatures, and its properties evolve with time and depend on the waiting time t_w after the quench. While glasses often behave like solids and have ubiquitous uses, the absence of a sudden structural change at T_g means that they are often viewed as frozen liquids.

The function $T_g(Q)$ depends on the quench rate Q and is defined as the temperature where the liquid leaves equilibrium [4–6]. As with aging, the glass/liquid relaxes towards equilibrium, and one can define a generalized $T_g(Q, t_w)$, $T_g(Q, t_w) > T_g(Q, t'_w)$ for $t_w < t'_w$. An alternative calorific glass transition temperature is frequently used, particularly by experimentalists (see, for example, Ref. [7]), and is defined by the change of the specific heat upon cooling from the liquid to the amorphous state. This definition of T_g does not coincide fully with the dynamic definition, but also shows aging effects. Careful measurements with modulated differential

scanning calorimetry (MDSC) can detect small changes of T_g after years of aging [8].

By contrast, mode coupling theory (MCT) for simple glasses predicts a transition at a critical temperature T_c some 20% above T_g . This temperature marks a transition from a flow dominated regime at higher temperatures to a region characterized by atomic hopping [9] and is related to the sharp increase of the viscosity often observed, particularly in “fragile” glasses [10]. Despite being originally designed for simple glasses, MCT behavior has been found in a large range of materials. A detailed review of the theoretical aspects of the glass transition can be found in Ref. [11].

Glasses are formed by substances as diverse as metals, polymers or biological materials [7,12] and Se glass is of special interest. It is the only glass containing a single element, and its predominantly chain structure places it at the boundary between polymer and network glasses. Its extensive literature includes recent reviews [13,14]. The dynamics of disordered Se has been studied by classical molecular dynamics (MD) [15,16], Monte Carlo [17–19], density functional methods [20–24], and methods that combine experiment and computer simulation for specific problems [25]. Density functional methods are often free of adjustable parameters, but are limited even with modern computers to a few hundred atoms and times of up to ns. This limits their applicability to high temperatures if one aims to describe relaxation and aging reliably.

Classical MD allows us to study the dynamics for longer times (μ s) and samples of thousands of atoms. The reliability of the results for specific materials depends crucially on the choice of interaction potential. We use here the three-body interaction derived by Oligschleger *et al.* [26], which was derived to reproduce the structures of small clusters and properties of the trigonal and α -monoclinic crystals. We focus here on the aging time dependence of simple quantities, including energy, volume and diffusivity, as well as the relaxation of the intermediate self scattering function (ISSF) and the nearest-neighbor bonds. The aging relaxation towards equilib-

^{*}h.schober@fz-juelich.de

rium is commonly described by a Kohlrausch-Williams-Watts (KWW) [27,28] stretched exponential expression. While this expression gives a good fit over long times, the physical origin of the stretching remains disputed, and the time transformation $t \rightarrow t + t_w$ is not clear. KWW expressions have been derived for a number of relaxation models, see Ref. [3] for a review. In multicomponent glasses with strongly differing dynamics of the components, the stretching exponents for the relaxations of atomic energy and volume have been found to differ [29]. Recent experiments found that for long times relaxations no longer follow a KWW law but a simple exponential one [30].

In our previous work on aging of a binary Lennard-Jones (LJ) glass [31], we have shown that the relaxation of a number of properties can be understood in terms of the aging of the instantaneous atomic mobility and the subsequent evolution of the mean square displacement (msqd). This description satisfies the $t \rightarrow t + t_w$ transformation requirements and in the long-time limit the relaxation law becomes exponential. A much slower relaxation of volume and enthalpy than of diffusivity was found. The present work aims to show the more general validity of these results by simulating Se, a glass from a different class of materials, and to extend it to additional properties. In the present investigation, we use constant pressure (NPT) ensembles instead of the constant volume (NVT) ones in the previous work, which shows that the results do not depend on the details of choice of ensemble in the simulation. Since we are interested in the medium to long-time aging the starting ensembles were not produced by a rapid quench from a much higher temperature [32] but by a slower quench of rate $Q_r = 10^{11}$ K/s. In the LJ glass, we found the atomic mobility as the only determining factor for aging. In the following, we refer to this as diffusive relaxation channel. Se has strong covalent bonds and one expects the rearrangement of these bonds without diffusion as a second relaxation mechanism, a nondiffusive relaxation channel.

II. SIMULATION

We have performed MD simulations at fixed pressure (NPT ensemble) for ten independent systems of $N = 5488$ atoms with periodic boundary conditions. The calculations were done on the JURECA computer at FZ-Jülich utilizing an “in house” program used earlier in previous work by Caprion *et al.*, e.g., Ref. [33]. The temperature was adjusted by velocity scaling and the pressure by the Parrinello-Rahman algorithm [34]. The equations of motion are integrated with a velocity Verlet algorithm [35] with a time step of 1 fs. The volume mass parameter was set to $W = \sqrt{Nm_{\text{Se}}}$, where m_{Se} is the mass of the Se atom. A small volume damping term was added to reduce volume fluctuations at high temperatures. The interatomic interaction of Se was simulated by the three-body potential of Oligschleger *et al.* [26], whose parameters had been adjusted to reproduce properties of Se clusters [36] and the trigonal and α -monoclinic allotropes, including geometries, energies, and phonon spectra [37,38]. This interaction model has been useful in a range of contexts [6,16,33,39–45], and its high-temperature results agree well with a recent density functional study using 600 atoms [24]. The interaction model does not distinguish between intra- and

interchain interactions, and it reproduces the experimental structure factor and pair correlation function at room temperature (see Sec. VIA). Density and temperature deviate by a few percent from the experimental values. This could be rectified somewhat by adjusting the length and energy parameters of the interaction, but this was not carried out here, so that present and earlier works are compatible. The results are compared with experiment in Sec. VIII.

First, the ten samples were equilibrated at $T = 650$ K and then quenched by reducing the velocities at each time step (1 fs) corresponding to 0.001 K down to $T = 420$ K and 0.0001 K below. Figure S7 in Ref. [46] shows the evolution of the instantaneous temperature for one sample. The quench rate measured by the reduction of the mean temperature was $\approx 4 \times 10^{11}$ K/s down to $T = 420$ K and $\approx 4 \times 10^{10}$ K/s below. The slower quench rate covers the temperatures most relevant in the present work. We then chose quenched configurations near the temperatures used in the aging study. The configurations used were taken all at the same quench time. This means there was a distribution of initial instantaneous temperatures spanning about 5 K. Subsequently the configurations were rapidly quenched to the exact desired temperature. Properties were then monitored for up to 800 ns, depending on temperature. Figure S8 in Ref. [46] shows for one sample at $T = 290$ K the distributions of initial velocities for the as quenched state and after aging for 300 ns. The shift of the maximum reflects the temperature drop from the instantaneous temperature of $T = 297$ K of the as quenched sample to $T = 290$ K during aging. Otherwise no statistically relevant change is seen. To check for possible effects of the velocity scaling procedure additional runs at constant energy, i.e., without any velocity scaling, were done. These did not show any significant effect, due to system size and smallness of the rescaling. To check for possible size effects, additional samples with 49392 and 148176 atoms were simulated at $T = 350$ and 500 K. No significant effect was seen in the evolution of the atomic energy and volume or the structure factor, see Figs. S9–S11 in Ref. [46].

Data were collected at intervals of typically 1 to 10 ps, and results were averaged when deemed necessary over time spans that were negligible compared with the aging time. Aging was studied as usual as a function of waiting time, t_w , i.e., the time between reaching the desired temperature in the original quench and the time when properties (e.g., volume and energy) were measured, or the starting time for the measurement of bond breaking and intermediate self-scattering function (ISSF). Our aim is to understand aging over long times, and short time aging, typically less than a picosecond, was not studied in detail. The lowest temperature ($T = 270$ K) was dictated by computing requirements, and the highest ($T \approx 500$ K) by the chosen quench rate and the merging of ballistic and diffusional effects.

III. AGING AND RELAXATION

The dynamics of liquids and glasses exhibit relaxations both above and below the glass transition. In equilibrium these relaxations are on average independent of time. Quantities like volume and energy at a given temperature T are constant and the dynamics, as a simple example the mean

square displacement (msqd) $\langle s^2(t) \rangle$, depends only on the time t elapsed from the start of the measurement, but not on the waiting time t_w before the measurement started. This holds no longer for unequilibrated systems. For example, the atomic volume V taken at a time t depends on t_w the time the observation started. Obviously $V(T, t_w, t) = V(T, t'_w, t')$ for $t_w + t = t'_w + t'$ holds for the evolution of the volume and other quantities that measure the state of the system as function of time. An exponential relaxation obeys this relation trivially. However, in experiments and simulations one finds a slowing down of the relaxation with time. This is often described by a Kohlrausch-Williams-Watt (KWW) stretched exponential expression. Without an additional dependence of the prefactor on t_w , a KWW law violates the $t + t_w$ invariance.

Our previous work on aging of a binary Lennard-Jones glass [31], a model for a metallic glass, showed that aging is closely related to diffusion. The relaxation of the glass after the quench was driven by diffusion over distances of about a nearest-neighbor distance, and the diffusional mobility (diffusivity) of the atoms decreased during aging. This can be understood as the annihilation of local structures that favor mobility, which can be described for long times by a linear rate equation. At the temperatures investigated, nonlinear effects would have to be taken into account for times of typically less than 1 ps. The magnitude of these nonlinear effects depends on the details of the production process, and they were not studied in detail. In the present work, we follow the previous approach for the diffusivity and its effect on the aging of the properties of the glass. By construction, the expressions obey the $t + t_w$ -invariance condition.

Unlike most metallic glasses, Se has strong covalent bonds. In addition to the diffusive relaxation in the simple metallic glass, some of these bonds break during relaxation. This can be triggered by diffusion when Se atoms of different chains come close and chains reconnect, but we show below that additional bond breaking occurs that does not show the signature of diffusion.

We study here the relaxation (aging) for long times, and the figures show the aging of different properties for $T = 290$ K. Figures for other temperatures are given in the separate sections and/or the summary, as appropriate. We study first the elementary processes diffusion and bond breaking. The change of the ballistic motion/vibration with aging has little influence on the long time behavior and is not studied in detail.

IV. DIFFUSION

The equilibrium diffusion coefficient can be determined from the long time limit of the atomic mean square displacement (msqd)

$$D_\infty(T) = \frac{1}{6} \lim_{t \rightarrow \infty} \langle s^2(t) \rangle_T, \quad (1)$$

where $s(t)$ denotes the atomic displacement and $\langle \dots \rangle_T$ indicates averaging over atoms and ensembles at temperature T . If the melt or amorphous material relaxes to an equilibrium, $D_\infty(T)$ depends only on temperature T . If no such equilibrium is reached, $D_\infty(T)$ depends on the production history. At the temperatures considered here this dependence is small

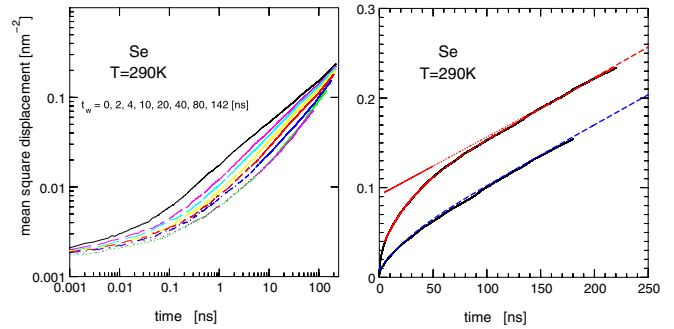


FIG. 1. (Left) Mean square displacement at $T = 290$ K for waiting times up to 142 ns in double logarithmic representation. (Right) Mean square displacement in linear representation. As quenched samples, $t_w = 0$, top and aged samples ($t_w = 40$ ns) bottom. Solid black lines: simulation result, dashed red and blue lines: fit with Eq. (4), and dotted red line: msqd calculated from D_∞ .

and of minor importance. The msqd at finite times, however, strongly depends on the production history as well as on temperature. To make this effect tractable in aging studies, one generally adopts a common starting point, normally a quench to the required temperature T followed by aging of the samples at this T . After a waiting time t_w , we investigate the aging of various properties, i.e., their dependence on t_w .

To study the aging effects on diffusion, we introduce a time-dependent diffusion coefficient (diffusivity) $D(T, t_w, t)$, which converges to $D_\infty(T)$ in the limit $t \rightarrow \infty$

$$D(T, t_w, t) = \frac{1}{6} \frac{d}{dt} \langle s^2(t_w, t) - s_{\text{ball}}^2(t_w) \rangle_T. \quad (2)$$

Here, $s_{\text{ball}}(t_w)$ accounts for displacements due to ballistic and/or vibrational motion, shown, for example, in Fig. 1 as the value at $t = 1$ ps. The ballistic term depends slightly on t_w , mainly due to the dependence of the boson peak [47] on aging, but this effect is negligible here. Equation (2) applies only for times beyond the ballistic regime. A different definition of the time-dependent diffusion coefficient is often used:

$$\begin{aligned} D_{\text{integral}}(T, t_w, t) &= \frac{1}{6t} \langle s^2(t_w, t) - s_{\text{ball}}^2(t_w) \rangle_T \\ &= \frac{1}{6t} \int_0^t D(T, t_w, t') dt'. \end{aligned} \quad (3)$$

Both experiment and simulations show that the diffusivity $D(T, t_w, t)$ decreases with t , and the apparent diffusion constant $D_{\text{integral}}(T, t_w, t)$ and the msqd at time t are reduced with increasing waiting time t_w . We have shown [48] that this decrease with aging of the diffusion coefficient of a binary Lennard-Jones glass can be described a defect-type model,

$$D(T, t_w, t) = D_\infty(T) + D_{\text{def}}(T) c_{\text{def}}(T, t_w) \exp(-\alpha_D(T)t). \quad (4)$$

For different waiting times the concentrations are related by $c_{\text{def}}(T, t_w) = c_{\text{def}}(T, t'_w) \exp(-\alpha_D(T)(t_w - t'_w))$. Such a description is widely used, e.g., to describe defect annihilation in radiation experiments. Here “defect” does not relate to a specific defect type but to unspecified deviations from the (quasi)equilibrium structure of the melt or glass reached after

long aging times. These defects enhance the diffusion, and the decay of their concentration is treated in linear approximation by a rate equation that should hold after a short run-in time. After a rapid quench, the glass can be too far from equilibrium to be treated by a linear rate equation, but Eq. (4) holds after the fast initial relaxation. The initial “defect” concentration reflects strongly the production history of the system, including the quench rate and the waiting time before the measuring commences.

The decay constant α_D , however, changes only weakly with history. The mean square displacement (msqd) follows from Eqs. (2) and (4) as

$$\begin{aligned} & \langle s^2(t_w, t) - s_{\text{ball}}^2 \rangle \\ &= 6t \left[D_\infty + \frac{D_{\text{def}} c_{\text{def}}(t_w)}{\alpha_D} (1 - \exp(-\alpha_D t)) \right]. \end{aligned} \quad (5)$$

Here we have omitted the contribution of the plateau in the msqd, which becomes important at lower temperatures. At the temperatures of the present simulations, the plateau acts mainly as a small time shift that is negligible in the long-time aging. In the context of diffusional aging discussed below, it is important to calculate the waiting time dependence, i.e., the time t_x when the msqd reaches a given value. For times $t > 1/\alpha_D$, t_x changes exponentially with t_w , which is reflected in shifts of the bond breaking time discussed below (Fig. 5) and the decay time of the intermediate self-scattering function (Fig. 11).

As an example, Fig. 1 shows in a double logarithmic plot (left) the time evolution of the mean square displacement (msqd) at $T = 290$ K for waiting times of up to 142 ns. The msqd is recorded relative to the configuration of the sample after a waiting time t_w following the quench. The temperature is kept constant during the waiting time. As expected, the msqd for a given time decreases with waiting time before the start of the measurement, and the diffusivity of the Se atoms decreases with aging. For well-aged samples, at $T = 290$ K after a waiting time $t_w \approx 80$ ns, the msqd $s^2(t_w, t)$ becomes independent of t_w , and further aging has no visible effect. In this plot, the initial increase $\propto t^2$ due to ballistic motion and vibration is not resolved. The aging effects on these are not significant for the present investigation. For $t < 0.1$ ns, the plateau, typical for glasses is visible and becomes more pronounced with aging.

Figure 1 (right) shows that Eq. (4) provides an excellent fit to the diffusivity and the resulting msqd. The curves for the simulation results and the fit nearly coincide. It holds both for the as quenched system and the aged ones, e.g., after $t_w = 40$ ns. The values of D_∞ and α_D are independent of t_w , they do not change with aging. The dashed lines showing the fit are hardly distinguishable from the simulation results, shown by solid lines. The extrapolation from long times using D_∞ (straight line in the double logarithmic plot) shows the large effect of aging on the apparent diffusion, $D_{\text{integral}}(t_w, t)$. We do not observe an additional change of diffusivity on even longer timescales than the one given by $1/\alpha_D(T)$. Such a long-time change could be effected by even slower relaxations that necessitate the breaking of stable bonds. The effect on the diffusivity of the volume change during aging is small compared with the “defect aging” and can be neglected. The

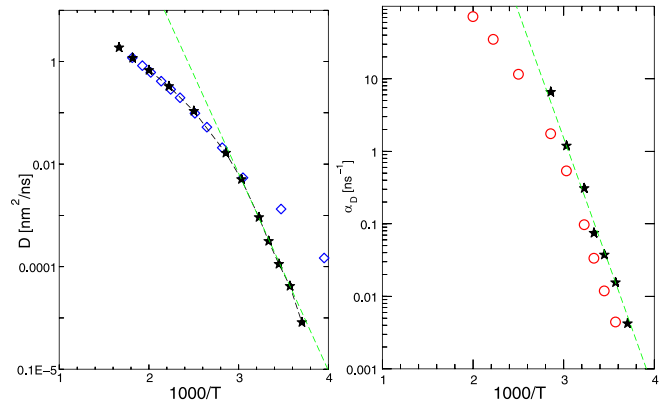


FIG. 2. Diffusion coefficient and its aging rate as functions of inverse temperature. (Left) Asterisks show $D_\infty(T)$ calculated from Eq. (4), dashed green line: Arrhenius fit for low temperatures, open diamonds: values from Ref. [16]. (Right) Asterisks show the aging rate $\alpha_D(T)$, dashed green line: Arrhenius fit for low temperatures, and open circles: long-time rate of rate of diffusion over nearest-neighbor distance, α_{NN} .

same was observed in the previous study of a Lennard-Jones glass [31]

By fitting the time dependence of the msqd with Eq. (4), the long-time diffusion coefficients $D_\infty(T)$ can be evaluated for lower temperatures when a direct calculation by Eq. (1) is ruled out by excessive computing demands. Figure 2(left) shows by (black asterisks) the diffusion coefficients $D_\infty(T)$ for temperatures above $T = 270$ K. For comparison we show (open diamonds) the values calculated for the same system with a quench rate of 10^{13} and equilibration times of 9 to 16 ns at each temperature [16]. As expected, the calculations agree at high temperatures when the quench rate is sufficiently low or the subsequent aging or observation time long enough. Below about $T = 330$ K, the long times of the earlier calculation are still insufficient, and the diffusivity is already overestimated by two orders of magnitude on cooling to 250 K. As the calculations agree at high temperatures, the fit of $D(T)$ by the mode coupling theory (MCT) [49] of the previous work holds. The high-temperature diffusion coefficient follows an MCT law $D(T) \propto (T - T_c)^\gamma$, with a critical temperature of about $T_c = 330$ K and $\gamma = 1.88$ [16]. Below that temperature, the diffusivity follows an Arrhenius law $D_\infty(T) = 2.23 \times 10^9 \times \exp(-8850/T)$ in units of nm^2/ns .

The value of $D_\infty(T = 500) = 0.677 \times 10^{-5} \text{ cm}^2/\text{s}$ agrees well with the neutron scattering result of Axmann *et al.* [50] ($\approx 0.4 \times 10^{-5} \text{ cm}^2/\text{s}$). Phillips *et al.* [51], however, give a much lower estimate ($\approx 2.2 \times 10^{-7} \text{ cm}^2/\text{s}$). A recent density functional calculation estimates $D(T = 500) = 0.096 \rightarrow 0.178 \times 10^{-5} \text{ cm}^2/\text{s}$.

The aging rate $\alpha_D(T)$ is shown in the right part of Fig. 2. Like the diffusion coefficient itself it can, at low temperatures, be fitted by an Arrhenius law $\alpha_D(T) = 4.4 \times 10^{10} \times \exp(-8026/T)$. The exponent is about 10% lower than the corresponding one in $D_\infty(T)$. This means that the aging times of the diffusion coefficient increase not as fast as $D_\infty(T)$ with cooling. For comparison we also show the long-time rate of diffusion over a nearest-neighbor distance

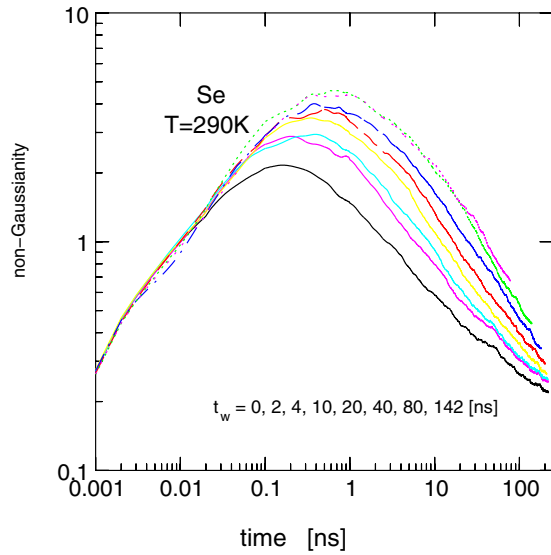


FIG. 3. Increase of the non-Gaussianity parameter $\alpha_2(t)$ at $T = 290$ K with increasing waiting time $t_w = 0, \dots, 142$ ns, curves from bottom to top.

R_{NN} .

$$\alpha_{NN}(T) = 6 * D_{\infty}(T) / R_{NN}^2. \quad (6)$$

These values are less than $\alpha_D(T)$ by more than a factor of 3. After an initial fast relaxation for times $t < 1$ ps, the Se atoms move on average less than a nearest-neighbor distance during the aging time $1/\alpha_D$ of $D(T)$.

A. Dynamic heterogeneity

The dynamic heterogeneity (DH) is a typical “glassy” property. In a high-temperature liquid, the dynamics is nearly homogeneous, and all atoms are equally mobile. An undercooled liquid is still homogeneous when averaged over long times, but at intermediate times atoms or groups of atoms differ in their mobility; some are slow, others fast. Over long times, slow atoms convert to fast atoms and vice versa, an effect called dynamic heterogeneity. The timescale for this conversion increases with cooling. Upon cooling to the glass transition this heterogeneity increases dramatically. It affects all dynamic properties e.g. vibration [52] where it is connected to quasi-localized modes or the viscosity [53]. The DH is often studied by using four point correlation functions [54]. DH is observed most easily in the msqd and the atomic diffusivity. A common measure is the non-Gaussianity parameter (NGP) α_2 [55]

$$\alpha_2(t) = \frac{3\langle \Delta s^4(t) \rangle}{5\langle \Delta s^2(t) \rangle^2} - 1. \quad (7)$$

The NGP is normalized to $\alpha_2(t) = 0$ for homogeneous vibrations and diffusion. The temperature and time dependence of $\alpha_2(t)$ for our system has been reported earlier [40], and we focus here on the change during aging, as exemplified for $T = 290$ K. Figure 3 shows the evolution of the NGP with time for different waiting times t_w . After a small increase due to the inhomogeneity of the vibrations, not shown here, the NGP increases $\propto \sqrt{t}$ for all waiting times. This increase

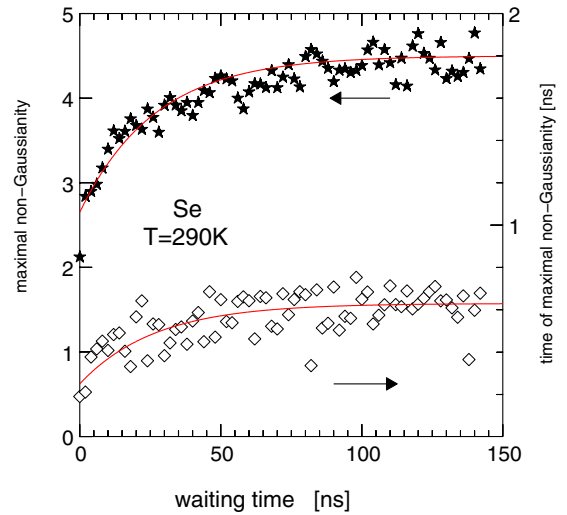


FIG. 4. Waiting time dependence of time and value of the maximal non-Gaussianity. Red lines: fit with an exponential aging rate α_D determined from the aging of the diffusivity, Eq. (4).

with \sqrt{t} is seen also in the previous study of the temperature dependence of the NGP. It can be explained as a signature of collective motion, i.e. groups of atoms move collectively [40]. In the present case such collective motion is to be expected due to the chain structure. The NGP then passes through a flat maximum and finally decays. For the well-aged samples, the decay is approximately $\propto t^{-2/3}$. The NGP decays more slowly for shorter waiting times, an effect of the interplay of the increase of $\alpha_2(t)$ with aging and the decay for long times. The increase of the NGP with aging is similar to the one with cooling, see Ref. [40] and Fig. S2 in Ref. [46]. The NGP of the as-quenched samples corresponds roughly to the one at $T = 320$ K after aging. Therefore the as quenched samples can be assigned a heterogeneity temperature $T_{\text{heterogeneity}} \approx 320$ K. Aging reduces this temperature by 30 K.

As observed for the LJ glass [48], the aging rate of the NGP is the same within the error bars as that of the diffusivity $\alpha_D(T)$. This holds for both the value and time of the maximal $\alpha_2(t)$, see Fig. 4. At $T = 290$ K, the maximal NGP increases by a factor 2 upon aging. Cooling further to $T = 270$ K this factor increases to 3. For a different quench procedure, these values will of course differ. However, the aging constants and the general trend will still hold.

B. Diffusion-driven aging

Diffusion and non-Gaussianity are essentially single particle properties, and their aging can be described by the annihilation of “defects” during the transition to a more ideal glass structure. The relaxation of extensive quantities—such as energy, volume, or pressure—is much slower for a metallic like system [31], but it is driven by diffusion, and the time dependence can be explained by the evolution of the mean square displacement that reflects the aging of the diffusion coefficient. There are then two timescales for aging in an LJ glass: a shorter one for diffusivity and heterogeneity, given by Eq. (4), and a longer one for energy, pressure, and volume. These timescales begin to diverge near the critical

temperature. As seen above the shorter timescale can be expressed by a defect annihilation process, whereas the second is related to diffusion-driven aging and given by the msqd (diffusive aging).

The aging of some quantity $A(T, t, t_w)$ is described by

$$\begin{aligned} A(T, t, t_w) &= A_\infty(T) + \Delta A(t_w) e^{-\langle s^2(t, t_w) - s_{\text{ball}}^2 \rangle / \ell_A^2(T)} \\ &= A_\infty(T) + \Delta A(t_w) e^{-6D_{\text{integral}}(t, t_w)t / \ell_A^2(T)}. \end{aligned} \quad (8)$$

Here, $\Delta A(t_w)$ denotes the initial deviation from the long-time limit and depends on the production procedure and waiting time. The length ℓ_A is characteristic for the aging of the quantity A . It indicates how far, on average, an atom diffuses during the aging time $t_{\text{aging}}^A(t_w)$. We expect it to be of the order of the nearest neighbor distance and independent of t_w . For long times, $D_{\text{integral}}(t, t_w) \rightarrow D_\infty(T)$, aging becomes exponential, and the limiting aging time is given by the diffusion coefficient. Upon cooling the diffusion coefficient (and the aging rate) will eventually decrease exponentially with decreasing temperature. The enhanced diffusivity for shorter times causes a faster aging at those times, often described by stretched exponential (KWW) expressions. From Eq. (8) we can define two different aging times, the standard one by the decay of the aging effect to $1/e$, t_{aging}^A , and a second one, $t_{\text{aging}, \infty}^A$, for the limit of long-time aging that is determined by $D_\infty(T)$. t_{aging}^A depends on the initial state, but $t_{\text{aging}, \infty}^A(T)$ does not. Since the diffusivity decreases with time one always has $t_{\text{aging}}^A < t_{\text{aging}, \infty}^A$. The aging times are given by

$$\ell_A^2(T) / \langle s^2(t_{\text{aging}}^A, t_w) - s_{\text{ball}}^2 \rangle = 1 \quad (9)$$

and

$$t_{\text{aging}, \infty}^A(T) = \ell_A^2(T) / (6D_\infty(T)), \quad (10)$$

respectively.

V. BOND BREAKING

In a strongly covalent material such as Se, one expects additionally to the timescale due to atomic mobility a second one given by the breaking of the covalent bonds. Bond breaking can be triggered by diffusive motion but also occurs nondiffusively. In an ideal Se crystal, each atom has covalent bonds to two nearest neighbors. In amorphous Se one expects a similar nearest-neighbor number per atom. Taking the usual definition of nearest neighbor, namely, each atom closer than the distance of the first minimum of the pair correlation function $g(r)$, $r < r_{\text{min}}$, we find an average nearest-neighbor number of $n_{\text{NN}}(0) = 2.05$, nearly independent of aging. Since $g(r_{\text{min}})$ does not vanish, this number depends slightly on the choice of cutoff, but this does not influence the following discussion. To investigate the waiting time dependence of bond breaking, we determine the nearest neighbors of each atom at waiting times t_w and follow the evolution of the neighborhood. The chain structure is changed locally, even when the average number of nearest-neighbor bonds changes little with time: individual bonds are broken, nearest-neighbor pairs break up, and new pairs are formed.

The solid lines in Fig. 5 (left) show the time decay of the original neighbor bonds for different waiting times. Comparison with Fig. 1 shows that this decay is slower than the

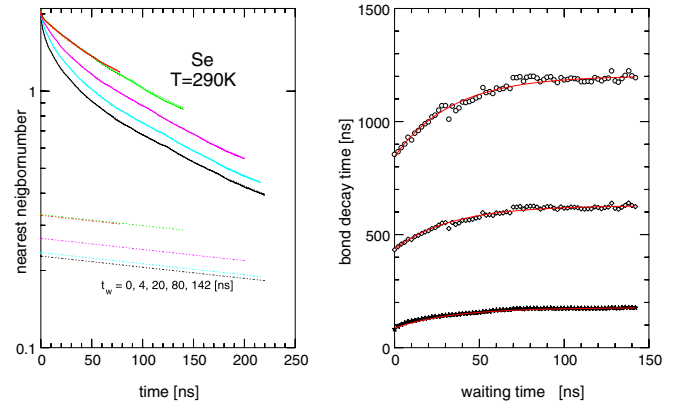


FIG. 5. (Left) Decay of the initial nearest-neighbor bonds per atom (double counting of bonds) $n_{\text{NN}}(t, t_w)$, for waiting times $t_w = 0, 4, 20, 80, 142$ ns (from bottom to top). Solid lines simulation results, and hardly distinguishable dashed lines fit with Eq. (11). Dotted lines at bottom: exponential decay of bonds not affected by diffusion. (Right) Change of bond decay times with waiting time. From bottom to top: decay to $1/e$, 0.1, and 0.05 of initial value, respectively. The red line indicates an exponential fit.

slowing down of the atomic mobility (diffusivity), which follows Eq. (4). We describe this decay by two terms: a decay driven by diffusion according to Eq. (8) and an additional exponential decay describing the nondiffusive breakup of bonds. The decay of the nearest-neighbor number is then

$$\begin{aligned} n_{\text{NN}}(T, t, t_w) &= n_{\text{NN}}(T, 0, t_w) \exp(-\alpha_{\text{bb}}(T)t) \\ &\times [f_{\text{bb}}(T, t_w) + (1 - f_{\text{bb}}(T, t_w)) \\ &\times \exp(-\langle s^2(t, t_w) - s_{\text{ball}}^2 \rangle / \ell_{\text{bb}}^2(T))]. \end{aligned} \quad (11)$$

Here $n_{\text{NN}}(T, 0, t_w)$ denotes the average nearest-neighbor coordination number present initially. The dependence on T and t_w is slight and unimportant for the present results. Each nearest neighbor bond is then counted twice. $n_{\text{NN}}(T, t, t_w)$ denotes the average number of original connections present at time t , $f_{\text{bb}}(T, t_w)$ gives the fraction of bonds not broken by a diffusive process, $\alpha_{\text{bb}}(T)$ is the nondiffusive bond-breaking rate, and $\ell_{\text{bb}}(T)$ is the characteristic length for diffusive bond breaking. With $\ell_{\text{bb}} = 0.338$ nm, it is slightly larger than the nearest-neighbor distance and independent of t_w . The fit by Eq. (11) (dashed lines in Fig. 5) shows that the curves are nearly indistinguishable. Most bonds break with a diffusive process, and the fraction of other bonds $f_{\text{bb}}(T, t_w)$ increases from an initial 10% to 15% with increasing waiting time (dotted lines). $f_{\text{bb}}(T, t_w)$ depends on production history and aging.

Figure 5 (right) shows the increase of the bond breaking times with aging, from bottom to top decays to $1/e$, 0.1, and 0.05, respectively. Except for the initial value for the as-quenched glass, the increase of the decay time can be fitted by an exponential law

$$t_{\text{bb}}(T, t_w) = t_{\text{bb}}(T, t_w \rightarrow \infty) - \Delta t_{\text{bd}}(T) \exp(-\alpha_{\text{bb}} t_w). \quad (12)$$

The aging time $1/\alpha_{\text{bb}}$ for bond breaking is much shorter than the bond-breaking time itself (note the different timescales in Fig. 5, left and right). It is comparable to the aging time of

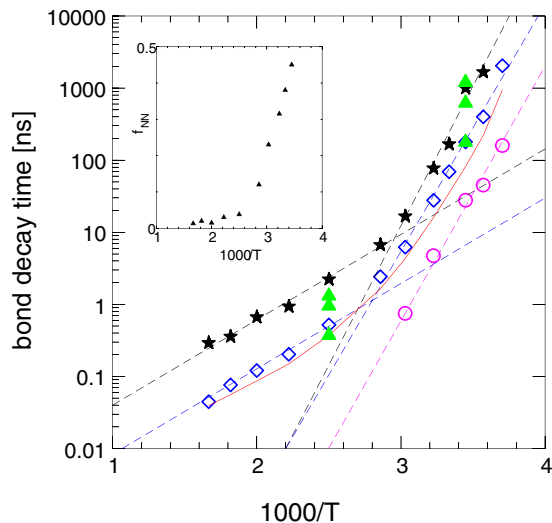


FIG. 6. Decay times of the nearest-neighbor bonds as function of inverse temperature. For large waiting times ($t_w \rightarrow \infty$), the times (inverse rates) for the decay to $1/e$ of nondiffusive and diffusive parts of the bond decay are shown by asterisks and blue diamonds, respectively. The red line shows the decay time for the as quenched samples. The green triangles show for two temperatures and well aged samples the times for a bond decay to $1/e$, 0.1 , and 0.05 of their respective original values. The open magenta circles give the aging times $1/\alpha_{bb}$ of the rates for bonds to decay to $1/e$. The dashed lines show the Arrhenius approximations for the various decay times. The insert shows the fraction f_{bb} of the bonds decaying nondiffusively in aged samples.

the diffusion coefficient. At $T = 290$ K the same exponent, $\alpha_{bb} = 0.29 \text{ ns}^{-1}$ reproduces the values for decays down to 5% . This results from the small contribution of the nondiffusive decay channel. For lower temperatures the nondiffusive decay gains importance, insert in Fig. 6, and the exponential fit of the decay times requires different exponentials, depending on the final fractions.

Since at all temperatures the relative weight of the two decay channels changes with production history and waiting time the bond breaking time will do likewise. Furthermore, the relative weights of the two channels also change with the definition of decay time, i.e., the slower nondiffusive channel becomes more important when one asks for a larger fraction of bonds to be broken. The decay time of the diffusive channel reaches its maximal value in the limit of long aging times ($t_w \rightarrow \infty$): $\ell_{bb}(T)/(6D_\infty(T))$. These times are shown by blue diamonds in Fig. 6. The characteristic length $\ell_{bb}(T)$ increases with temperature from 0.32 nm at $T = 270 \text{ K}$ to 0.49 nm at $T = 400 \text{ K}$. For the nondiffusive channel no marked change of the rate with aging was observed. The times, shown by black asterisks, are always larger than their diffusive counterparts. The temperature dependencies of both times follow approximately Arrhenius laws with a change of activation energy at about 340 K . The approximate activation energies are 7900 and 2700 kT for the diffusive channel and 8900 and 2700 kT for the nondiffusive channel, respectively. Lowering the temperature the nondiffusive bond breaking gains in importance. The insert of the figure shows as function of

inverse temperature the fraction of the bonds that are broken via a nondiffusive mechanism in the aged samples. Below $T = 350 \text{ K}$, this mechanism rapidly gains in weight and eventually dominates.

A bond lifetime, defined by the decay of the original bonds to some fraction f_{unbroken} is influenced more strongly by the slower nondiffusive channel the smaller f_{unbroken} . We illustrate this for well aged samples at two temperatures by green triangles. At $T = 290 \text{ K}$, the decay of the bond number to $1/e$ is dominated by the diffusive channel whereas the decay to 5% is dominated by the slower nondiffusive one. At $T = 400 \text{ K}$, the diffusive process always dominates. The bond breaking in not fully aged samples is faster than given by the limiting values. The red line in Fig. 6 shows bond decay time to $f_{\text{unbroken}} = 1/e$ for the as quenched samples.

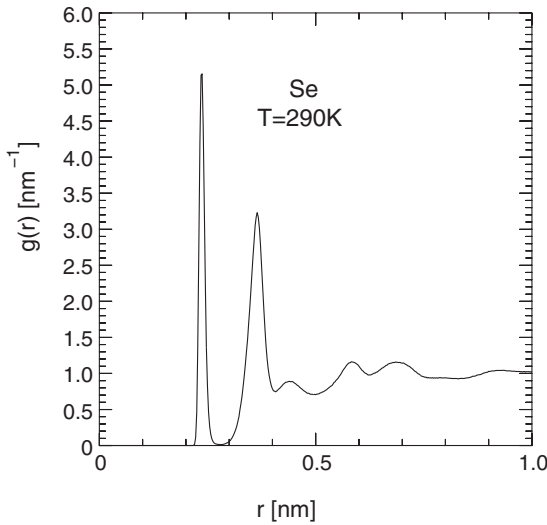
Finally we show by red circles in Fig. 6 the aging times, as expressed by Eq. (12), for decays of the bonds to a fraction $1/e$. The aging times are about an order of magnitude shorter than the corresponding bond-breaking times. They follow an Arrhenius law with an activation energy of 8100 kT , similar to the aging times of the diffusivity. This confirms that the aging of the bond-breaking rate is initially dominated by diffusion which inhibits a flip flop of bonds.

VI. AGING OF ONE-TIME FUNCTIONS

Properties such as structure factors, energy or volume are determined by the state of the system at a given time. In the context of aging, they depend on the production process and the subsequent waiting time, and one needs to determine the value after some time t and not how it has evolved. An example is the instantaneous diffusion coefficient (diffusivity) $D(T, t_w, t)$ discussed above. Other quantities, such as mean square displacements, bond breaking dynamics, or intermediate scattering functions, quantify the evolution over given time intervals and are two-time functions. The evolution history determines ultimately the one-time properties, and $D(T, t_w, t)$ is given by the msqd at time t without showing the previous history. We look first at the aging of typical one-time functions.

A. Structure

Amorphous Se is formed by chains and rings of Se atoms. Using a cutoff distance of 0.28 nm at $T = 350 \text{ K}$, we find 18% of the atoms in rings and 82% in chains of varying lengths. As definition of ring we take here a loop of atoms that do not have a third atom within the cutoff distance. This means no threefold coordinated atoms are in the loop. Five-membered rings make up about half of the ring atoms, the others being distributed over larger rings with 6, 7, 8, and more atoms (15% , 9% , 13% , and 13% , respectively). These numbers agree semiquantitatively with those of a density functional calculation [24]. The experimental situation concerning ring and chain structure is unclear [24]. Apart from the earliest stages of aging, changes in the number of atoms forming rings were insignificant, but there was a small change in the distribution of ring sizes. It is difficult to determine if this is a random fluctuation or a true aging effect. 93.5% of the atoms are twofold-, 6% threefold-, and 0.4% singly coordinated. Depending on

FIG. 7. Pair correlation function of Se at $T = 290$ K.

the connectivity at threefold coordinated atoms different chain lengths can be defined. We have not investigated this further, but have focused on the pair pair correlation factor (PCF) $g(r)$ and static structure factor (SSF) $S(q)$.

The strong aging of the mobility is not reflected in these simple quantities used to identify structure. The PCF in an isotropic system is defined as

$$g(r) = \frac{V}{4\pi r^2 N^2} \left\langle \sum_i \sum_{j \neq i} \delta(r - r_{ij}) \right\rangle, \quad (13)$$

where r_{ij} is the distance between atoms i and j and $\langle \dots \rangle$ denotes the configurational average. Independent of aging, the PCF (Fig. 7) shows a well separated first neighbor peak, reflecting the ideal coordination number 2 of Se, and a well defined peak for the second neighbors. The integral up to the minimum between the first two maxima gives a coordination number of 2.05 for our amorphous samples. The positions of the first three peaks at 0.235, 0.364, and 0.443 nm lie within the experimental ranges reported in the literature [56,57]. No marked change with aging was discernible within the numerical accuracy of this calculation. This could be different for a more brutal quench program, e.g. an instantaneous quench from significantly higher temperatures. We focus here on long-time aging effects when the fast initial aging after such a rapid quench would have decayed. Short time effects following a rapid quench depend more on the details of the sample preparation. No attempt was made to follow the evolution with waiting time t_w of the minuscule change of $g(r)$.

There are slightly larger aging effects on the static structure factor $S(q)$, which we calculated by direct Fourier transform using q vectors compatible with the periodicity. This avoids artifacts due to cutoffs of $g(r)$ at large r when using the Fourier transform of the PCF.

$$S(q) = 1 + \frac{1}{N_q N} \left\langle \sum_{|\mathbf{q}|=q} \sum_i \sum_{j \neq i} \exp(-i\mathbf{q}(\mathbf{R}_i - \mathbf{R}_j)) \right\rangle, \quad (14)$$

where N_q denotes the number of \mathbf{q} values with $|\mathbf{q}| = q$.

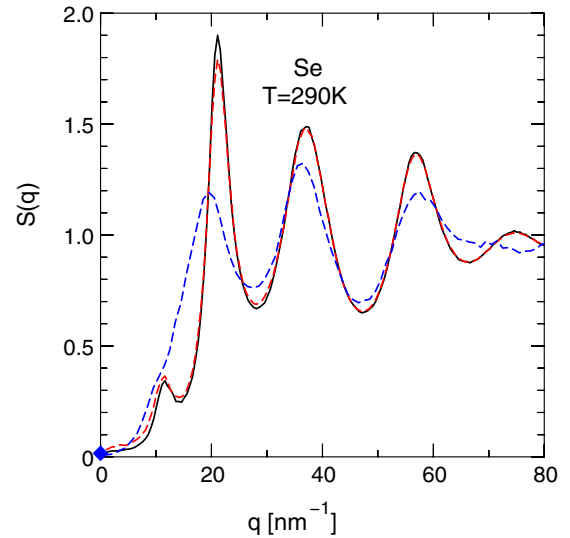


FIG. 8. Static structure factor, $S(q)$, at $T = 290$ K; dotted red line: as quenched, solid black line: after a waiting time of 219 ns. The blue diamond indicates the long wave length limit calculated from the experimental compressibility [58] and density and the dashed blue line gives the neutron scattering results at $t = 293$ K [56].

As an example we show $S(q)$ at 290 K in Fig. 8. The calculated SF agrees well with the one derived from neutron scattering [56] and the peak positions agree with the reported experimental ones [59,60]. With increasing temperature the peaks broaden but shift little. During aging the first main peak grows by about 5%. This growth is compensated by a deepening of the first minimum. No aging effect is seen at higher q . As shown in Fig. 9, the increase of $S(q)$ with waiting time is compatible with an expression analogous to the one for $D(T, t_w, t)$ Eq. (4),

$$S_{\max}(T, t) = S_{\max}(T, t = \infty) - \Delta S_{\max} \exp(-\alpha_D t), \quad (15)$$

where $S_{\max}(T, t = \infty)$ is the final, long time, value, ΔS_{\max} is the deviation at the start of the observation, and α_D is the decay constant determined from the diffusivity. The small variation with time, combined with the strong scatter of the data, prohibits a definite conclusion. Since the total number of nearest-neighbor bonds stays constant during aging, we do not expect bond breaking effects without diffusion to be

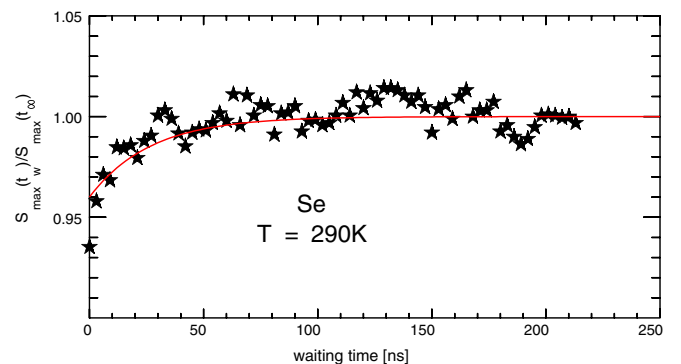


FIG. 9. Waiting time dependence of the height of the first peak of the structure factor. The red line shows the fit by Eq. (15).

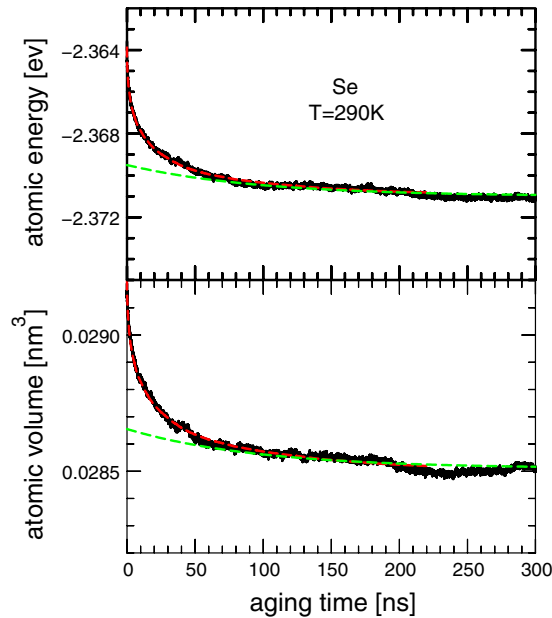


FIG. 10. Decrease of the atomic energy (top) and volume (bottom) with time; black: simulation result, red lines: fit by Eq. (16), green dashed lines: fit of the long-time relaxation using the long-time diffusion coefficient $D_{\infty}(T)$.

prominent in the aging of the structure factor. The contribution of nondiffusional bond breaking is very small.

As in earlier simulations a prepeak is seen at around $q = 10 \text{ nm}^{-1}$ that has been ascribed to correlations between holes in the structure [16,61]. The prepeak vanishes under high pressure, indicating the removal of holes by compacting. The prepeak intensity also diminishes during aging, and we interpret this as a signature of the annihilation of holes. This is consistent with the shrinking of the atomic volume discussed below. The experimental curve shows a slight shoulder, not a prepeak, which may be a resolution effect.

B. Volume and energy

The effect of aging on the atomic volume and energy is more pronounced than in the PCF and structure factor. At $T = 290 \text{ K}$, the atomic volume shrinks from an initial, as quenched value of 0.0292 nm^3 to a long time limit of 0.0285 nm^3 . The corresponding values for the energy are -2.364 eV and -2.372 . This means that in our system with $N = 5488$ about 130 atomic volume units are annealed by aging on average. This value is of course strongly dependent on the production history or quench rate. What part of this “free volume” is localized in voids or spread out is not clear.

In our previous work on the LJ glass [31], we found that the atomic volume and energy age on much longer timescales than the diffusivity. Energy and pressure aged in parallel, and the aging could be understood as driven by diffusion. This also holds in the present case, see Fig. 10. The relaxation with aging of both volume and energy is reproduced very well by diffusivity aging, Eq. (8):

$$E(T, t_w, t) = E_{\infty}(T) + \Delta E(t_w) \times \exp(-6D_{\text{integral}}(t_w, t)t/\ell_{E,V}^2(T)),$$

TABLE I. Lengths in nm for diffusional bond breaking, decay of the ISSF, and aging of volume and energy.

T (K)	ℓ_{bb} (nm)	$\ell_{E,V}$ (nm)	ℓ_{ISSF} (nm)
270	0.31	0.28	0.17
280	0.31	0.26	0.17
290	0.35	0.26	0.17
300	0.36	0.26	0.17
310	0.39	0.22	0.17
330	0.43	0.25	0.17
350	0.49	0.21	0.17

$$V(T, t_w, t) = V_{\infty}(T) + \Delta V(t_w) \times \exp(-6D_{\text{integral}}(t_w, t)t/\ell_{E,V}^2(T)). \quad (16)$$

The simulation results (black lines) and the fit results (red lines) are nearly indistinguishable. To show the effect of the aging of the diffusivity, we show (green dashed lines) a fit to the long time relaxation using in Eq. (16) the long-time diffusion coefficient $D_{\infty}(T)$ instead of the time dependent $D_{\text{integral}}(t_w, t)$. This shows that when the diffusivity reaches its equilibrium at around $t = 70 \text{ ns}$ the aging of energy and volume follows a simple exponential law $\exp(-\alpha t)$ with $\alpha = 6D_{\infty}(T)/\ell_{E,V}^2(T)$. The characteristic length scale is for both energy and volume $\ell_{(E,V)} = 0.255 \text{ nm}$, i.e., approximately the nearest-neighbor distance. It does not change markedly between $T = 270$ and 350 K , Table I. The length $\ell_{(E,V)}(T)$ is about 25% shorter than its counterpart seen in bond breaking, $\ell_{bb}(T)$. One would expect an additional contribution to the relaxation by the bond breaking not coupled to diffusion. If present, it is too small to be observed in the evolution of energy and volume. This might be explained by the fact that the total number of nearest-neighbor bonds does not change markedly during aging. A linear relation between enthalpy and volume relaxation, as follows from Eq. (16), has been observed also in an experimental relaxation study over 10^5 s [62].

In the binary LJ glass, which is often studied as a model of a simple glass that follows the predictions of mode coupling theory [63], a pronounced cusp of $\ell_{(E,V)}(T)$ was seen near the mode coupling temperature [31]. In the present case, we do not see such a cusp.

VII. INTERMEDIATE SELF-SCATTERING FUNCTION

In the evolution of properties such as the volume or energy t and t_w are interchangeable. Some properties change very little, including the static structure factor and the coordination number. More insight is gained by studying the dynamics, i.e., the evolution of some property with time, starting at a time t_w the result depends on both t_w and t . At the temperatures used in this investigation, the glasses exhibit considerable change of the dynamics as shown, e.g., in Fig. 1 if one concentrates on the evolution of msqd itself instead of using it merely to calculate the diffusion coefficient. Also in the study of bond breaking we have seen a marked change of the dynamics, not only an aging dependence of the bond decay time (Fig. 5).

A commonly used tool to gain information about the dynamics in glasses and liquids is the intermediate

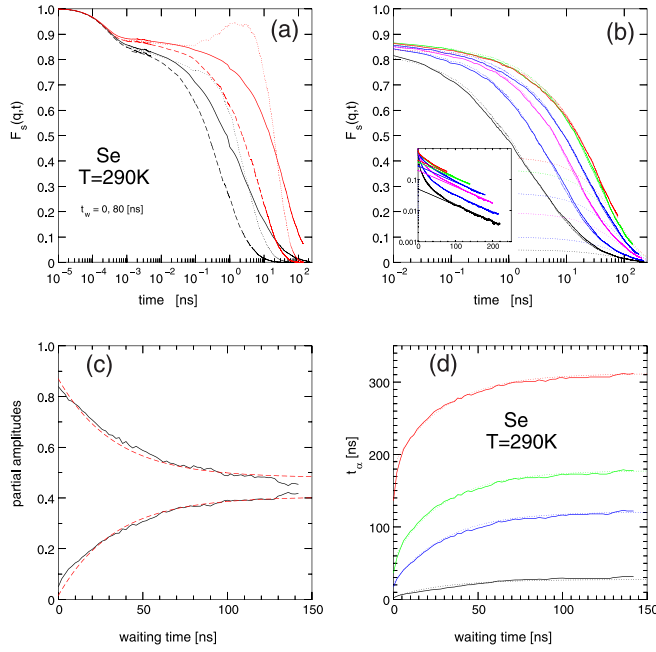


FIG. 11. Intermediate self-scattering function, $F_s(q, T)$, of Se at $T = 290$ K and $q = 21.1 \text{ nm}^{-1}$. (a) Solid lines $F_s(q, T)$ for the as-quenched samples (black) and after a waiting time of $t_w = 80$ ns (upper red line); dashed lines: Gaussian approximation; dotted lines: expansion including lowest order non-Gaussianity. (b) Decay of the intermediate scattering function on a logarithmic timescale for waiting times $t_w = 0, 4, 20, 80,$ and 142 ns (from bottom to top). The simulation results (solid lines) and the fit with Eq. (19) (dotted) are hardly distinguishable. Lower dotted lines indicate the exponential decay for long times. Using a linear timescale, the insert emphasizes the long-time logarithmic decay. (c) Waiting time dependence of the amplitudes in Eq. (19), lower line: $A_{F,I}(t_w)$, upper line: $A_{F,d}(t_w)$, dotted line exponential approximation to $A_{F,I}(t_w)$. (d) Relaxation times as function of waiting time. From bottom to top: decay of the ISSF to $1/e, 0.1, 0.05, 0.01$.; dotted lines: exponential approximation of long-time aging.

self-scattering function (ISSF)

$$F_s(q, t) = \frac{1}{N} \left\langle \left[\sum_i e^{i\mathbf{q}\mathbf{r}_i(t)} \right] \left[\sum_i e^{i\mathbf{q}\mathbf{r}_i(0)} \right] \right\rangle, \quad (17)$$

where $\langle \rangle$ indicates the average over angles and configurations. The ISSF can be extracted experimentally by various scattering techniques, e.g., incoherent neutron scattering. Its time decay divides into three regimes. At the shortest times ($t < 0.1$ ps), not treated here, $F_s(\mathbf{q}, t)$ decays rapidly due to ballistic and vibrational motion. At about 1 ps this decay is fully evolved. At long times, $F_s(\mathbf{q}, t)$ decays to zero on timescales of a few picoseconds in the hot liquid, a few nanoseconds in the undercooled liquid and finally the timescale diverges in the glass as $T \rightarrow 0$. This decay is associated with the α relaxation. A shoulder or plateau related to the β relaxation evolves for intermediate times in the undercooled liquid and even more strongly in the glassy state.

Figure 11(a) shows $F_s(q, t)$ for q corresponding to the first main peak of the static structure factor, $S(q)$. It shows the usual behavior both for the as quenched samples and after

a waiting time of 80 ns. In the ballistic/vibrational regime, $t < 0.3$ ps, little aging effect is discernible. This is in agreement with the absence of major aging effects on both $g(r)$ and the average number of nearest neighbor bonds. The shoulder following the ballistic regime becomes more pronounced with aging, and stretches to about 1 ns for the aged samples. The strongest effect is seen in the α -relaxation regime where the relaxation time increases by orders of magnitude during aging.

The short time behavior of the ISSF can be described by expanding the exponential in Eq. (17) [3,64]

$$F_s(q, t) = \exp\left(-\frac{q^2 \langle s^2(t) \rangle}{6}\right) \times \left[1 + \frac{1}{2} \left(-\frac{q^2 \langle s^2(t) \rangle}{6}\right)^2 \alpha_2(t) + \dots \right]. \quad (18)$$

The first (Gaussian) term describes fully homogeneous dynamics. It describes the vibrational part adequately, but fails already for the onset of the shoulder [dashed lines in Fig. 11(a)]. The vibrational non-Gaussianity is relatively small and changes little during aging, Fig. 3. The second term accounts in lowest order for the dynamical heterogeneity as expressed by the non-Gaussianity coefficient α_2 . It extends the validity of the expansion to about 100 ps, covering the main part of the shoulder of $F_s(q, t)$ (dotted lines). The evolution of the shoulder is strongly aging dependent, as also seen for the non-Gaussianity itself (see Fig. 3). Following the ballistic/vibrational regime for all waiting times, the NGP increases as $\alpha_2(t) \propto \sqrt{t}$. This universal increase has been found [40] to be independent of temperature. The change of the height of the shoulder is, therefore, given by the strong dependence of $\langle s^2(t, t_w) \rangle$ on the waiting time. The time when $F_s(q, t)$ breaks from the shoulder correlates with the time when $\alpha_2(t)$ breaks from $\alpha_2(t) \propto \sqrt{t}$. The formation of the shoulder (plateau) can thus be traced to the heterogeneity. The extent of the shoulder is given by the breakaway from the \sqrt{t} -increase towards the maximum of $\alpha_2(t)$. The variation in height reflects the decrease of the short time mean square displacement with aging.

The expansion of $F_s(q, t)$ breaks down for times of order ns and beyond. The NGP passes its maximum around 1 ns and is strongly affected by aging. At this point, the time-dependence of the msqd is still dependent on aging and is not yet linear. To study this time regime in more detail, Fig. 11(b) shows $F_s(q, t)$ (solid lines) for a number of waiting times in a logarithmic-linear plot as in (a) and a linear-log plot as insert. An expression analogous to Eq. (11) gives an excellent fit for all waiting times (dashed) lines that is hardly discernible from the simulation result.

$$F_s(q, t, t_w) = \exp(-\alpha_{\text{ISSF}} t) [A_{F,\text{nd}}(T, t_w) + A_{F,d}(T, t_w)] \times \exp(-\langle s^2(t, t_w) \rangle / \ell_{\text{ISSF}}^2). \quad (19)$$

This implies that two distinct mechanisms drive the decay of the ISSF, one driven by diffusion and a second by nondiffusive bond breaking. The two factors in the exponent, $1/\alpha_{\text{ISSF}} = 83$ ns and $\ell_{\text{ISSF}} = 0.167$ nm, are independent of t_w , whereas $A_{F,\text{nd}}(T, t_w)$, $A_{F,d}(T, t_w)$, and the msqd vary with aging. The length ℓ_{ISSF} is again somewhat less than the nearest-neighbor distance and is shorter than its counterparts in the volume and energy relaxation, $\ell_{E,V}$, and in the bond breaking, ℓ_{bb} . The

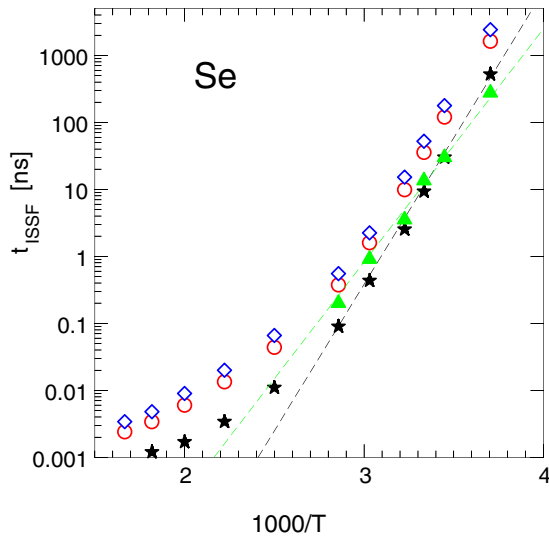


FIG. 12. Temperature dependence of the decay and aging times of the intermediate self-scattering function (ISSF) at $q = 21.1 \text{ nm}^{-1}$. Black asterisks decay of the ISSF to $1/e$, red circles to $1/10$, blue diamonds decay to $1/20$. The green triangles indicate the aging time of the decay time. The dashed lines show the Arrhenius laws for the lower temperatures.

insert in Fig. 11(b) shows the long time exponential decay of the ISSF. The exponential contribution given by Eq. (19) is shown by dotted lines. Fig. 11(c) shows the increase of the nondiffusive contribution to the ISSF with aging and the concomitant drop of the diffusive contribution. The waiting time dependence of $A_{F,nd}(T, t_w)$ follows an exponential law

$$A_{F,nd}(T, t_w) = 0.405 - 0.39 * \exp(-t_w/33). \quad (20)$$

The decay of the ISSF is frequently used to define a relaxation time. In Se, where at least two distinct mechanisms with different timescales contribute to the decay, the relative importance of the mechanisms depends on the definition of the relaxation time. In Fig. 11(d), the waiting time dependence of the relaxation time is shown for decays to $1/e$, 0.1 , 0.05 , and 0.01 . The time dependence for long waiting times can be described by a simple exponential law

$$t_{\text{ISSF}}(t_w, f) \approx t_{\text{ISSF}}(0, f) + \Delta t_{\text{ISSF}}(f) \exp(-t_w/t_{\text{ISSF}}^{\text{aging}}), \quad (21)$$

where f denotes the fraction to which the ISSF has decayed. At $T = 290 \text{ K}$, the aging time $t_{\alpha, \text{aging}} = 30 \text{ ns}$ is independent of f and similar to the aging time of the nondiffusional amplitude. This indicates that the main aging mechanism for the ISSF is the shift from diffusive to nondiffusive decay, in agreement with the similarity of the aging times of the ISSF and the diffusivity ($1/\alpha_D = 27 \text{ ns}$).

The decay with time of the ISSF and its aging time are summarized for temperatures from 600 to 270 K in Fig. 12. The decay times t_{ISSF} for decays to $F_s(q, t, t_w) = 1/e$, 0.1 , and 0.05 are indicated by black asterisks, red circles, and blue diamonds, respectively. Below 300 K , the decay follows an Arrhenius law

$$t_{\text{ISSF}}(T, t_w \rightarrow \infty) = 2.81 \times 10^{-14} \exp(-10000/T) \text{ ns}, \quad (22)$$

shown (dashed line) for the decay to $1/e$. The decay to lower values shows a similar decay rate. The fast decay for the as-quenched sample is not covered by this law. In the case of $T = 290 \text{ K}$ the Arrhenius law is valid for times larger than 10 ns , see Fig. 11(d). The decay times for “as-quenched” samples will in general be shorter and depend on the exact history.

The aging time, $t_{\text{ISSF}}^{\text{aging}}(T)$ of $t_{\text{ISSF}}(T, t_w)$ is shown by green triangles (for decay to $1/e$). For low temperatures, it is less than the corresponding $t_{\text{ISSF}}(T)$, at higher temperatures this is reversed. $F_s(q, t, t_w)$ decays to $1/e$ before the corresponding aging time is reached. Note that the aging effect here is always taken relative to the sample with $t_w = 0$. In the limit $t_w \rightarrow \infty$, the effect of aging vanishes and the “incomplete” aging becomes irrelevant. At low temperatures the aging time again follows an Arrhenius law (dashed),

$$t_{\text{ISSF}}^{\text{aging}}(T) = 2.910 \times 10^{-11} \exp(8000/T) \text{ ns}. \quad (23)$$

The aging of the ISSF and the bond breaking time at the lower temperatures follow the same Arrhenius law as the aging of the diffusion coefficient, which suggests strongly that they have a common origin.

VIII. COMPARISON WITH EXPERIMENT

Comparisons with experiment have been given in several places above. In summary, the calculated PCF and SF compare well with experiment and the long wave length limit of the SF agrees with the one calculated from the experimental compressibility and density. The experimental values for the diffusion coefficient vary greatly, but the calculated value lies in the range of both experiment and the density functional calculation.

The distributions of rings and chains was not studied systematically in this work. The present results agree semi-quantitatively with those of the recent density functional calculation [24]. One obvious result is the dominance of five membered rings in particular over eight membered ones. Experimental studies concentrated mainly on the fraction of atoms in chains versus eight membered rings. The difference between the Raman active modes in trigonal Se (A_1 , 233 cm^{-1}) and monoclinic Se (250 cm^{-1}) has been interpreted as the signature of eight-membered rings in the glass [65]. It was found that the relative fraction of chain- and ring atoms changes with temperature [47]. It was reported that the chain-, ring- structure changes, even on a scale of months [8], which far exceeds the timescale of any simulation. However, Se_5 , Se_6 , and Se_7 molecules are more prevalent in the vapor above liquid Se [66], pointing to their presence in the liquid.

The interaction model used was constructed to fit small molecules and crystalline allotropes. Small deviations of the predicted values for the density and temperature variation have to be expected. These should not affect the basic mechanisms of aging that are the subject of this paper. Figure 13 shows that at room temperature the calculated density as quenched is about 7% higher than the experimental one. Aging increases this discrepancy. This is probably mainly due to limitations of the interaction model and could be reduced somewhat by a rescaling of the length parameter. This would not change the present conclusions and has not been carried

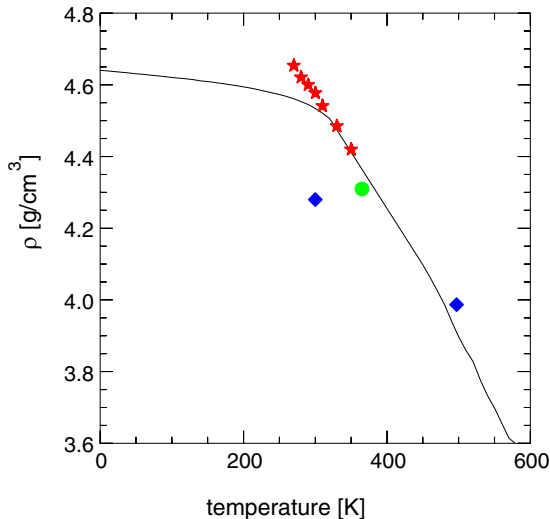


FIG. 13. Temperature dependence of the density: black line density after the quench; red asterisks final density after aging ($\rho_\infty(T)$) according to Eq. (16); blue diamonds experimental density [67,68]; and green circle density after aging of expanded sample, see text.

out, so remaining consistent with earlier simulations with this model interaction.

The absence of larger voids that are suppressed by the periodic boundary conditions is another possible effect, and Andonov [57] estimated that they comprise 10% of the volume at room temperature. To check for their presence, we have performed an additional run with $N = 148176$ under constant energy conditions (NPE), starting from the relaxed NPT sample at $T = 350$ K. All lengths were scaled by 1.03% and the evolution of volume/density was monitored for 4.5 ns. The final state, shown by a green circle in Fig. 13, was at a temperature of 366 K with a density of 4.31 g/cm³. This change is in the right direction, but is not conclusive. Even this large sample is small on experimental scales and would suppress larger voids in the glass.

The calculated thermal volume expansion coefficient in the liquid $\alpha_V = 3.4 \pm 0.1 \times 10^{-5} \text{ K}^{-1}$ agrees reasonably well the experimental value $\alpha_V = 3.5 \pm 0.01 \times 10^{-5} \text{ K}^{-1}$ [69,70]. Approaching T_g the calculated coefficient reduces to about $\alpha_V \approx 2.1 \times 10^{-5} \text{ K}^{-1}$ (taken between 350 and 400 K).

We are not aware of experimental data which allow a quantitative comparison of the aging data. In particular, a simultaneous measurement of diffusion and properties such as volume relaxation would be useful.

IX. SUMMARY

In addition to a rapid initial relaxation on a picosecond scale, we have identified three mechanisms in relaxation and aging in the temperature range from $T = 270$ –500 K, spanning the glass transition of Se. These are a slowing down of the atomic mobility, a relaxation driven by diffusion, and a decay of remaining nearest-neighbor bonds. The first two were identified previously for the “metallic” LJ glass [31] and the present results confirm and expand these findings. In addition to the first two effects, bond breaking without accompanying diffusion could be seen in the time dependence

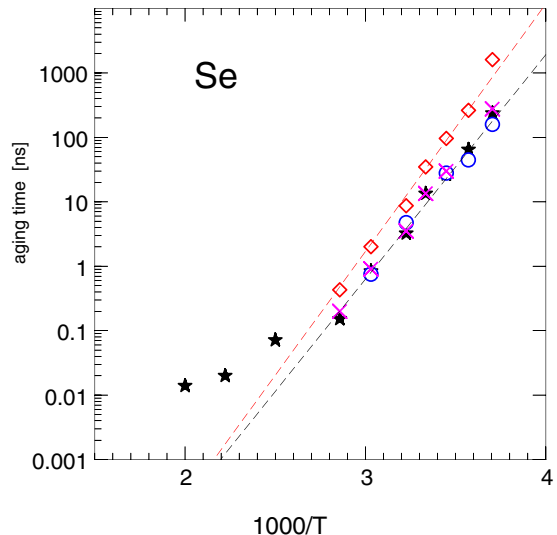


FIG. 14. Temperature dependence of typical aging times. Black asterisks: aging of the diffusion constant, red diamonds: long-time aging of atomic volume and energy, blue circles: aging of the bond breaking time, and magenta crosses: aging of the decay time of the ISSF. The dashed lines indicate the Arrhenius laws for the aging time $1/\alpha_D$ of the diffusion coefficient (black) and of $6D_\infty(T)/\ell_{E,V}^2(T)$ (red).

of the bond breaking itself and the decay of the ISSF but not in the volume and energy relaxation. This might be different for glasses whose dynamics are more strongly affected by covalent bonding.

We summarize in Fig. 14 the temperature dependence of typical aging times, i.e., the time for the long-time aging to decay to $1/e$. The aging time of the diffusivity $1/\alpha_D$ is shown by black asterisks. As shown in Sec. IV, it follows below about 300 K an Arrhenius law $1/\alpha_D(T) = 2.27 \times 10^{-11} \times \exp(8026/kT)$ ns. The aging of the bond breaking time and the decay time of the ISSF are shown by blue circles and magenta crosses, respectively. They follow below 300 K the aging of the diffusion constant as demonstrated for $T = 290$ K above. This shows that, once the diffusion constant has aged, so have the relaxation times of diffusion-driven relaxations. By contrast, the relaxation of volume and energy are much slower. After a sufficient waiting time, their aging is dominated by $D_\infty(T)$ [Eq. (16)], not by the aging of the instantaneous diffusion coefficient [Eq. (4)]. Apart from a small variation of $\ell_{E,V}$ (Table I), volume and energy aging below 300 K slow down exponentially with the low temperature law of the diffusion coefficient $D_\infty(T)$, apart from possible small contributions due to bond rearrangement seen in long time experiments [8].

Figure 14 shows that diffusion dominates in the aging process near T_g . It also illustrates the difference in aging toward an infinite time equilibrium structure [seen in the aging of $E(T, t_w)$ and $V(T, t_w)$] and the aging of the decay time of a correlation function (bond decay, ISSF) whose decay is dominated by atomic motion. Table I gives the lengths for the diffusional relaxation processes. These lengths are of the order of the nearest-neighbor distance. We find no temperature variation of ℓ_{ISSF} and a moderate lowering of $\ell_{E,V}$ with increasing

TABLE II. long-time limits of diffusional aging time $1/\alpha_D$, diffusional decay time ($\ell^2/6D_\infty$), and non-diffusional decay $f_{bb}(\infty)$ and $1/\alpha_{ISSF}$, limiting fraction of nondiffusional decay $f_{bb}(\infty)$ and $A_{F,nd}(\infty)$, decay times for the as-quenched samples [$t_{bb}(0)$ and ($t_{ISSF}(0)$)] and long-time aged samples [$t_{bb}(\infty)$ and ($t_{ISSF}(\infty)$)], and α -relaxation time t_α for $t_w \rightarrow \infty$. All times in nanoseconds.

T (K)	bond decay						ISSF					
	$1/\alpha_D$	$\ell_{bb}^2/6D_\infty$	$f_{bb}(\infty)$	$1/\alpha_{bb}$	$t_{bb}(0)$	$t_{bb}(\infty)$	$\ell_{ISSF}^2/6D_\infty$	$A_{F,nd}(\infty)$	$1/\alpha_{ISSF}$	$t_{ISSF}(0)$	$t_{ISSF}(\infty)$	t_α
270	237	2000	>0.35	10^4	9.9		600	>0.36	>1000	190		
280	64.5	400	0.3	1700	230	490	115	>0.34	220	4.8	>62	125
290	26.7	180	0.23	1000	83	177	40	0.39	83	2.5	27.5	38
300	13.4	69	0.17	170	35	63	15	0.38	25	1.07	8.6	12
310	3.24	27	0.16	77	16	22	5.1	0.31	(8)	0.59	2.7	3.6
330	0.84	6.2	0.12	6.2	4.3	4.7	0.93	0.25	(11)	0.22	0.37	0.51
350	0.15	2.4	0.06		1.7	1.7	0.28			0.06	0.09	0.14
400	0.071	0.52			0.37	0.37				0.01	0.01	0.018
450	0.02	0.20			0.15	0.15				0.004	0.004	0.005
500	0.01	0.12			0.09	0.09				0.002	0.002	

temperature. The more rapid increase in the corresponding value for bond decay may reflect the larger probability for bonds to reconnect at higher temperatures, provided that the atoms do not move too far apart.

Table II collates typical times for bond decay and ISSF and compares them with the decay time $1/\alpha_D$ of the diffusion coefficient after the fast initial drop. We have seen that the aging of the diffusion coefficient is faster in the limit of long time aging than the diffusive decays of bond correlation and ISSF, which in turn are faster than the nondiffusive decays.

$$1/\alpha_D(T) < \ell_x^2(T)/6D_\infty(T) < 1/\alpha_x, \quad (24)$$

where x denotes bb and ISSF, respectively. The contribution f_x of the nondiffusive channel increases strongly as the temperature is lowered. For the temperatures studied here, the decay times after long aging $t_{bb}(\infty)$ and $t_{ISSF}(\infty)$ are largely determined by the diffusive process. At lower temperatures the nondiffusive process increases in importance due to the increase of f_x , and this is also true if one considers instead of the decay to $1/e$ one to a lower fraction. The decay times after an arbitrary production history can be smaller by orders of magnitude, as shown by the decay times $t_x(0)$ for the as-quenched samples in Table II.

When comparing $t_{ISSF}(T)$ and $\ell_{ISSF}^2(T)/6D_\infty(T)$, it should be noted the former measures the decay from an initial value unity, while the latter includes only the decay after the initial ballistic/vibrational decay of $F_s(q, T)$. The decay from the value of $F_s(q, t)$ that follows the ballistic decay and an eventual decay from a plateau value is usually referred to as α -decay. Estimates of the decay time t_α are given in the last column of Table I. Ballistic decay is included by taking the value of $F_s(q, t)$ for $t = 1$ ps as the starting value for the α -decay. At 1 ps, the decay of $F_s(q, t)$ due to ballistic/vibrational motion is largely evident [see Fig. 11(a)]. The value shows the dominance of the diffusive channel in the α relaxation,

notwithstanding the takeover by the nondiffusive decay of $F_s(q, t)$ for longer times $t > t_\alpha$. At higher temperatures the simple separation into ballistic and α relaxation adopted here breaks down, particularly when t_α drops to the picosecond range.

X. CONCLUSIONS

There are three time domains for the aging of undercooled liquid and hot glassy Se. There is a rapid initial relaxation on timescales of picosecond that depends strongly on the quench history; it is stronger for larger quench rates. In the second stage, aging can be described by the annihilation of “defects,” i.e., local structures enhancing the atomic mobility, that can be described by a simple rate equation for the atomic mobility. Relaxation is driven by atomic diffusion, and the typical decay of the relaxation rate with time can be attributed to the aging of the diffusivity due to the “defect” annihilation. This accounts for the non-Arrhenius behavior.

For very long times, diffusional aging follows an Arrhenius law given by the equilibrium (infinite time) diffusion coefficient and a length that is of the order of the nearest-neighbor distance for all quantities studied here. The same scenario was observed previously for a simple metallic glass. An additional bond breaking occurs in Se that does not correlate with diffusion and affects the final stage of the ISSF decay. Nevertheless, aging of the ISSF is dominated by diffusion for the temperatures studied here. Since the diffusion coefficient in the glass drops exponentially with inverse temperature, the final aging slows exponentially as the temperature is lowered, and the aging time diverges when $T \rightarrow 0$.

ACKNOWLEDGMENTS

We thank R. O. Jones for numerous helpful discussions and acknowledge gratefully computing time granted through JARA-HPC (project jiff07) on the supercomputer JURECA at Forschungszentrum Jülich.

[1] I. M. Hodge, *J. Non-Cryst. Solids* **169**, 211 (1994).

[2] B. Ruta, E. Pineda, and Z. Evenson, *J. Phys.: Condens. Matter* **29**, 503002 (2017).

[3] M. Micoulaut, *Rep. Prog. Phys.* **79**, 066504 (2016).

[4] K. Vollmayr, W. Kob, and K. Binder, *Europhys. Lett.* **32**, 715 (1995).

- [5] J. Buchholz, W. Paul, F. Varnik, and K. Binder, *J. Chem. Phys.* **117**, 7364 (2002).
- [6] D. Caprion and H. R. Schober, *J. Chem. Phys.* **117**, 2814 (2002).
- [7] J. W. P. Schmelzer and I. S. Gutzow, *Glasses and the Glass Transition* (Wiley-VCH, Weinheim, 2011).
- [8] S. Dash, P. Chen, and P. Boolchand, *J. Chem. Phys.* **146**, 224506 (2017).
- [9] W. Götze and L. Sjögren, *Rep. Prog. Phys.* **55**, 241 (1992).
- [10] C. A. Angell, *Science* **267**, 1924 (1995).
- [11] L. Berthier and G. Biroli, *Rev. Mod. Phys.* **83**, 587 (2011).
- [12] *Glasses and Amorphous Materials*, edited by J. Zarzycki, Materials Science and Technology Vol. 9, edited by R. W. Cahn, P. Haasen, and E. J. Kramer (Wiley-VCH, Weinheim, 1991).
- [13] K. Tanaka, in *Amorphous Selenium and Nanostructures*, Springer Handbook of Glass, edited by J. D. Musgrave, J. Hu, and L. Calvez (Springer Nature Switzerland, Cham, 2019).
- [14] S. N. Yannopoulos, *J. Mater. Sci.: Mater. Electron.* **31**, 7565 (2020).
- [15] N. G. Almarza, E. Enciso, and F. J. Bermejo, *J. Chem. Phys.* **99**, 6876 (1993).
- [16] D. Caprion and H. R. Schober, *Phys. Rev. B* **62**, 3709 (2000).
- [17] C. Bichara, A. Pellegatti, and J.-P. Gaspard, *Phys. Rev. B* **49**, 6581 (1994).
- [18] J. C. Mauro and A. K. Varshneya, *Phys. Rev. B* **71**, 214105 (2005).
- [19] J. C. Mauro and A. K. Varshneya, *Phys. Rev. B* **72**, 024212 (2005).
- [20] D. Hohl and R. O. Jones, *J. Non-Cryst. Solids* **117-118**, 922 (1990); *Phys. Rev. B* **43**, 3856 (1991).
- [21] F. Shimojo, K. Hoshino, M. Watabe, and Y. Zempo, *J. Phys.: Condens. Matter* **10**, 1199 (1998).
- [22] F. Kirchhoff, G. Kresse, and M. J. Gillan, *Phys. Rev. B* **57**, 10482 (1998).
- [23] R. O. Jones, *Rev. Mod. Phys.* **87**, 897 (2015).
- [24] J. Kalikka, J. Akola, R. O. Jones, and H. R. Schober, *Phys. Rev. B* **102**, 104202 (2020).
- [25] M. García-Hernández, F. J. Bermejo, B. Fåk, J. L. Martínez, E. Enciso, N. G. Almarza, and A. Criado, *Phys. Rev. B* **48**, 149 (1993).
- [26] C. Oligschleger, R. O. Jones, S. M. Reimann, and H. R. Schober, *Phys. Rev. B* **53**, 6165 (1996). Parameter a in Table I should read 9281.2 and $\alpha = -7.9284$ instead of -7.984 .
- [27] R. Kohlrausch, *Pogg. Ann. Phys. Chem.* **167**, 179 (1854).
- [28] G. Williams and D. C. Watts, *Trans. Faraday Soc.* **66**, 80 (1970).
- [29] Y. Yu, M. Wang, D. Zhang, B. Wang, G. Sant, and M. Bauchy, *Phys. Rev. Lett.* **115**, 165901 (2015).
- [30] K. Niss, J. C. Dyre, and T. Hecksher, *J. Chem. Phys.* **152**, 041103 (2020).
- [31] H. R. Schober, *Phys. Rev. B* **85**, 024204 (2012).
- [32] W. Kob and J.-L. Barrat, *Phys. Rev. Lett.* **78**, 4581 (1997).
- [33] D. Caprion and H. R. Schober, *J. Chem. Phys.* **114**, 3236 (2001).
- [34] M. Parrinello and A. Rahman, *Phys. Rev. Lett.* **45**, 1196 (1980).
- [35] W. C. Swope, H. C. Andersen, P. Berens, and K. R. Wilson, *J. Chem. Phys.* **76**, 637 (1982).
- [36] D. Hohl, R. O. Jones, R. Car, and M. Parrinello, *Chem. Phys. Lett.* **139**, 540 (1987).
- [37] J. Donohue, in *The Structure of the Elements* (Wiley, New York, 1974), p. 370.
- [38] R. W. G. Wyckoff, in *Crystal Structures* (Krieger, Malabar, FL, 1982), p. 36.
- [39] C. Oligschleger and H. R. Schober, *J. Non-Cryst. Solids* **250-252**, 651 (1999).
- [40] D. Caprion, J. Matsui, and H. R. Schober, *Phys. Rev. Lett.* **85**, 4293 (2000).
- [41] C. Oligschleger and J. C. Schön, *J. Phys.: Condens. Matter* **9**, 1049 (1997).
- [42] T. Kosłowski, *Z. Phys. Chem.* **210**, 45 (1999).
- [43] C. Oligschleger, C. Facius, H. Kutz, C. Langen, M. Thumm, S. von Brühl, S. Wang, L. Weber, and J. Zischler, *J. Phys.: Condens. Matter* **21**, 405402 (2009).
- [44] A. H. Goldan, C. Li, S. J. Pennycook, J. Schneider, A. Blom, and W. Zhao, *J. Appl. Phys.* **120**, 135101 (2016).
- [45] A. Mukherjee, D. Vasileska, and A. H. Goldan, *J. Appl. Phys.* **124**, 235102 (2018).
- [46] See Supplemental Material at <http://link.aps.org/supplemental/10.1103/PhysRevB.103.094202> for plots for different temperatures. Additional plots show test results concerning the simulation procedure.
- [47] S. N. Yannopoulos and K. S. Andrikopoulos, *J. Chem. Phys.* **121**, 4747 (2004).
- [48] H. R. Schober, *Phys. Chem. Chem. Phys.* **6**, 3654 (2004).
- [49] W. Götze, in *Liquids, Freezing and the Glass Transition*, edited by J.-P. Hansen, D. Levesque, and J. Zinn-Justin (North Holland, New York, 1991).
- [50] A. Axmann, W. Gissler, A. Kollmar, and T. Springer, *Discuss. Faraday Soc.* **50**, 74 (1970).
- [51] W. A. Phillips, U. Buchenau, N. Nücker, A.-J. Dianoux, and W. Petry, *Phys. Rev. Lett.* **63**, 2381 (1989).
- [52] B. B. Laird and H. R. Schober, *Phys. Rev. Lett.* **66**, 636 (1991); H. R. Schober and B. B. Laird, *Phys. Rev. B* **44**, 6746 (1991).
- [53] H. R. Schober and H. L. Peng, *Phys. Rev. E* **93**, 052607 (2016).
- [54] L. Berthier, *Phys. Rev. E* **69**, 020201(R) (2004).
- [55] A. Rahman, *Phys. Rev.* **136**, A405 (1964).
- [56] F. Y. Hansen, T. S. Knudsen, and K. Caneiro, *J. Chem. Phys.* **62**, 1556 (1975).
- [57] P. Andonov, *J. Non-Cryst. Solids* **47**, 297 (1982).
- [58] A. K. Singh and G. C. Kennedy, *J. Appl. Phys.* **46**, 3861 (1975).
- [59] M. Edeling and W. Freyland, *Ber. Bunsen. Phys. Chem.* **85**, 1049 (1981).
- [60] K. Tamura and S. Hosokawa, *Ber. Bunsen. Phys. Chem.* **96**, 681 (1992).
- [61] S. R. Elliott, *J. Non-Cryst. Solids* **182**, 40 (1995).
- [62] P. Slobodian, P. Říha, R. W. Rychwalski, I. Emri, P. Sába, and J. Kubát, *Eur. Polym. J.* **42**, 2824 (2006).
- [63] W. Kob and H. C. Andersen, *Phys. Rev. E* **51**, 4626 (1995); **52**, 4134 (1995).
- [64] B. R. A. Nijboer and A. Rahman, *Physica* **32**, 415 (1966).
- [65] R. M. Martin, G. Lucovsky, and K. Helliwell, *Phys. Rev. B* **13**, 1383 (1976).
- [66] R. Steudel and E.-M. Strauss, in *Advances in Inorganic Chemistry*, edited by H. J. Emeleus and A. G. Sharpe (Academic Press, London, 1984), Vol. 28, pp. 135–166.
- [67] C. L. Yaws, *Chem. Eng. (New York)* **114**, 44 (2007).
- [68] Y. Tsuchiya, R. Satoh, and F. Kakinuma, *J. Non-Cryst. Solids* **250-252**, 468 (1999).
- [69] J. Bartoš, O. Šauša, P. Pustková, J. Šánělová, J. Křištiak, and J. Málek, *J. Non-Cryst. Solids* **351**, 1082 (2005).
- [70] J. Málek, R. Svoboda, P. Pustková, and P. Čičmanec, *J. Non-Cryst. Solids* **355**, 264 (2009).